

# Transmit Antenna Selection Based on Link-layer Channel Probing

Chen-Mou Cheng    Pai-Hsiang Hsiao    H. T. Kung    Dario Vlah  
 {doug, shawn, htk, dario}@eecs.harvard.edu  
 Harvard University  
 Cambridge, MA 02138

## Abstract

*In this paper, we propose transmit antenna selection based on receiver feedback of channel information obtained via link-layer probing. Furthermore, we report the performance gain of the proposed antenna selection scheme in an experimental multi-antenna 802.11 network. We built a low-altitude Unmanned Aerial Vehicle (UAV) testbed using commodity dual-antenna 802.11 hardware and performed field experiments to collect traces of link performance using antennas of various types and orientations. Based on the collected traces, we demonstrate that transmit antenna selection can achieve a significant amount of gain using a link-layer channel probing protocol at a relatively low probing rate. The largest improvement we observed with joint transmit/receive antenna selection in  $2 \times 2$  systems was 32%, about twice as much as that of receive-only antenna selection in  $1 \times 2$  systems, which achieved 17%. Moreover, a similar improvement is obtained with probing intervals up to about 200 milliseconds, which is infrequently enough to consume only a small fraction of the available 802.11 channel capacity. Since these results require only a low implementation and operational cost, we conclude that transmit antenna selection is a worthwhile technique to use with the kind of multi-antenna mobile ad-hoc networks we examined.*

## 1. Introduction

Antenna diversity is a well-known and commonly used technique for improving wireless communication performance. When multiple antennas are configured properly, they can take advantage of signals that traverse uncorrelated paths and thus compensate for the outages incurred in some of these paths. Several efforts have quantified the antenna diversity gain via the use of multiple antennas with proper polarizations or spatial separation [10]. Even in line-of-sight situations, the signal-to-noise ratio (SNR) gain can sometimes be as large as 12dB [3]. Furthermore, if the transmitter has knowledge of the channel state, then the channel capacity can be further increased by allocating more power to the transmit antennas with higher channel gain, a strategy known as the water-pouring or water-filling principle [7], [9]. To harness the diversity gain, complex and expensive radio-frequency (RF) circuitry is often required, e.g., for performing maximum ratio combining [8].

For the IEEE 802.11 wireless LAN (“Wi-Fi”), the use of multiple antennas has become easier in recent years due to

This material is based on research sponsored by Air Force Research Laboratory under agreement numbers FA8750-05-1-0035 and FA8750-06-2-0154. The U.S. Government is authorized to reproduce and distribute reprints for Governmental purposes notwithstanding any copyright annotation thereon. The views and conclusions contained herein are those of the authors and should not be interpreted as necessarily representing the official policies, either expressed or implied, of Air Force Research Laboratory or the U.S. Government.

the commercial availability of wireless LAN adapters equipped with dual antenna ports. These adapters use a switch to connect the antenna ports to only one set of RF transceiver circuitry. Moreover, such adapters implement receive antenna selection in the sense that they can detect the best receive antenna based on the signal strength measurements taken *within that packet’s preamble* [6]. As a result, the probability that the data portion of the packet is received on the better of the two antennas is increased.

Dynamic antenna selection could be especially important in mobile networks, where the nodes’ relative orientations change frequently. For example, in a scenario where a UAV with 802.11 communications capability is used for sensor data pickup or as a relay node, the maneuver of the aircraft due to turning or maintaining course could cause recurring changes in the relative positions in the radiation patterns of the communicating parties, as well as in the cross-polarization between the transmitting and receiving antennas [4], [5].

In this paper, we propose a transmit antenna selection scheme based on link-layer feedback from receivers on channel-probing packets. As a result, the sender can transmit packets on the antenna which, according to the feedback, yields better reception. We can use this transmit antenna selection together with receive antenna selection, which existing 802.11 hardware already supports.

Our evaluation of antenna selection consists of the following three units, which we present as the main contributions of this paper.

**1. Trace collection.** Via field experiments, we collected packet loss and signal strength data for constant bit rate (CBR) streams sent over 4 UAV antennas and received by 5 ground antennas. The resulting measurements describe 20 parallel channels in an outdoor environment under a mobility of about 40 miles per hour.

**2. Evaluation of antenna selection using emulation.** We built a multi-antenna channel emulator driven by pre-recorded packet traces, to do in-lab evaluation of antenna selection. Using the emulator, we evaluated the performance of a joint transmit/receive antenna selection implementation in the 60  $2 \times 2$  systems constructible from the  $4 \times 5$  channel traces obtained in step 1. We found that 1) within  $2 \times 2$  systems, the joint antenna selection always performs better than the individual single-antenna channels, 2) the best overall  $2 \times 2$  packet delivery rate (PDR) is 32% larger than the best overall single channel PDR, and 3) the best overall  $1 \times 2$  PDR under receive-only antenna selection is 17% larger than the best overall single-channel PDR. These results show not only that the joint antenna selection provides significant gain, but also that half of that gain is contributed by feedback-driven transmit antenna selection based on channel probing.

**3. Antenna selection field experiment.** We tested the step 2 antenna selection implementation in a  $2 \times 2$  UAV field experiment. We found that it was 6% better than with any single

antenna combination, though the sample variance was too high to draw definite conclusions. Even so, the measurements indicate that antenna selection works as could be expected based on the antennas’ radiation patterns and their positions.

## 2. Channel probing protocol (CPP)

We now present the Channel Probing Protocol (CPP), a simple link-layer protocol that we use to inform the transmit antenna selection. Every probing interval of  $T_P$  seconds, the transmitter sends a probe packet over alternating transmit antennas. The probe is received on the best antenna using the receiver’s hardware diversity circuit. The receiver feeds back to the sender the received signal strengths of the alternating probes, allowing the sender to choose the better transmit antenna to be used by subsequent packets. Figure 1 shows an example run of the protocol for three probing intervals between a transmit node A and a receive node B.

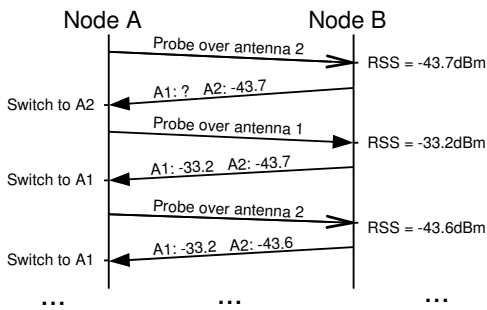


Fig. 1. An example CPP run. Labels  $A1$  and  $A2$  refer to the received signal strength of packets sent by  $A$ ’s antenna 1 or 2, respectively. Use of these antennas is indicated using solid and open arrows. Labels on the left side indicate the transmit antenna decision made using latest channel information fed back by node  $B$ . “RSS” stands for Received Signal Strength.

The sender’s probes and receiver’s reply packets can get lost over links with poor channel conditions. Channels under such conditions are not good candidates for communication anyway, so loss of their signal-strength information is not a serious problem. However, without up-to-date information about the bad channel conditions, the sender might use stale information obtained over a better channel. For this reason, the channel information expires after a certain timeout period, such as 5 probing intervals as we used in our implementation.

## 3. Trace collection

This section describes our trace gathering methodology and gives an overview of the collected data. We described a subset of these measurements and the methodology in a previous paper [4]. However, we did not address the issues of dynamic antenna selection in that previous paper. We begin by introducing our testbed, followed with a description of the antenna configurations. Lastly, we present the details of traffic patterns under observation and give a summary of the recorded data.

### 3.1. Testbed description

Our testbed consisted of a UAV node and 3 ground nodes. The ground nodes were placed on a line, with about 3 feet of separation between adjacent nodes. The nodes were powered by 400MHz AMD Geode single-board computers made by

Thecus Inc. Our UAV was based on the Senior Telemaster [1] model, a training model known for its stable flight characteristics. The UAV flew in oval-shaped laps passing directly over the ground nodes, at speeds of around 40 miles per hour. In these experiments, we used Atheros-chipset-based Wistron CM9 802.11a/b/g radio cards, with dual antenna ports and automatic receive antenna selection as described in Section 1. Each testbed node had two of these dual-antenna radio cards. Like some previous works [2], in order to avoid interference and association delays, we turned off the 802.11 IBSS protocol by switching the radios into “ad-hoc demo” mode.

We used two types of antennas on both the UAV and ground nodes. One was a 7-dBi, 2.4/5 GHz dual-band, omnidirectional antenna purchased from a commercial vendor (Netgate). The other was a half-wavelength 2-dBi dipole antenna built in-house. The main difference between these two antenna types is that the Netgate antenna produces an omnidirectional beam that is much narrower in the vertical plane than that of the dipole antenna.

### 3.2. Antenna configurations

Our testbed’s two antenna types were placed in a variety of orientations. In order to refer to these orientations in an unambiguous manner, we define the following of labels with respect to a level reference plane and a major axis that is either the direction of the runway for ground antennas, or that of the flight for UAV antennas:

$H$	horizontal dipole (i.e., dipole is parallel to the reference plane), orthogonal to the major axis
$H_N$	horizontal Netgate antenna, orthogonal to the major axis
$H_p$	horizontal dipole, parallel to the major axis
$V$	vertical dipole (i.e., dipole is orthogonal to the reference plane)
$V_N$	vertical Netgate antenna

We find it useful to specify the antenna orientations of multiple nodes at once. For this purpose, we introduce a notation for antenna configurations, which we define as pairs of antenna sets, and denote them as  $\{a_1, a_2, \dots, a_n\} \times \{b_1, b_2, \dots, b_m\}$ . The identifiers  $a_i$  and  $b_j$  are antenna labels. In each pair, the first set specifies the antennas on the UAV, while the second set specifies the antennas on the ground nodes. For example, the antenna configuration  $\{V, H\} \times \{V, V_N\}$  refers to a vertical and a horizontal dipole antennas on the UAV, while a vertical dipole and a Netgate antenna on the ground nodes. This notation will be sufficiently descriptive for our purposes without mentioning specific nodes or radios to which the antennas are attached.

The antenna configuration that we measured in the flight experiment was  $\{H_p, H_N, H, V\} \times \{V, H, H, V_N, H_p\}$ . The UAV carried two antennas per radio card. The ground nodes had just one antenna per card, leaving one antenna port unused. There was a total of 6 radio cards on the ground nodes, but we only use the measurements from 5 due to hardware issues with one radio card. We put up two  $H$  receivers to obtain additional data for  $\{H\} \times \{H\}$  systems, which were used in a co-located project regarding load-carry-and-deliver (LCAD) networking [5].

### 3.3. Description of traffic patterns

The UAV was the sole data transmitter during the experiments. It ran a user mode program that broadcast an endless stream of sequenced 320-byte UDP packets at the 6Mbps

modulation under 802.11a. At that rate, the transmission time of each packet was roughly  $500 \mu\text{s}$ . All radios were tuned to the same channel. The duration of the experiment was 14.7 minutes.

The sender enqueued packets in round-robin order to both of its radio cards. On each radio card, alternating packets were sent via alternating transmit antennas by the kernel driver. Since both input queues on each radio card were always full, the channel was never idle. However, the two radios contended for the medium using the standard 802.11 method with random backoff, so the actual output sequence was not perfectly alternating. We measured the resulting interleaving pattern in the lab and found that runs of packets from the same radio card had at most 7 packets, while their mean length was 1.53 packets. This means that the probing of different antenna combinations can still happen nearly at the same times.

The ground nodes received the broadcast packets using two radio cards. Each radio card used only a single antenna to receive the packets and record the transmit timestamp, sequence number, size, and the received signal strength indication (RSSI) value. (In Section 5, we will use the collected traces from two radio cards at a time to emulate the reception over the two antennas in receive antenna selection.) Therefore, from the data traces of just one ground node, we can obtain performance of 8 different links formed by the combination of 4 UAV and 2 ground node antennas. In general, an experiment with  $n$  UAV antennas and  $m$  ground antennas would let us measure the performance of  $nm$  links at once.

The key benefit of this multiplexing scheme is that we are able to measure multiple antenna combinations in a single UAV flight. This provides a more controlled experimental environment by eliminating signal variations due to, e.g., difference in flight trajectories and aircraft attitudes in several separate UAV flights. Moreover, we can evaluate the performance of all antenna combinations in essentially the same channel conditions. The average delay between two consecutive measurements using the same transmit antenna is merely 2.4 ms, which is short enough to regard the most influential physical parameters of the environment as constant. For example, given the speed of our UAV, it would take several hundreds of milliseconds for its bank angle to change enough to appreciably affect the receiver’s position in the antenna radiation pattern. Thus, we consider performance comparisons of antenna combinations, based on these collected traces, to be fair. We will use these traces to evaluate performance with respect to various metrics such as signal strength and packet loss rate.

#### 4. Trace-driven multi-antenna channel emulator

In order to evaluate antenna selection implementations quickly, we built a channel emulator driven by the pre-recorded traces. Recall that the traces are lists of entries containing the time, sequence number, size, and RSSI only of successfully received packets. For the purpose of emulation we inserted the missing entries corresponding to lost packets by interpolating the timestamps and sequence numbers of existing entries. The emulator receives packets from application processes, such as the CBR load and CPP implementation depicted in Figure 2, decides whether the packets should be dropped, and, if not, forwards them to receiving processes. Specifically, for a packet received at time  $T$ , the emulator decides using the first trace entry whose reception timestamp  $T_{\text{near}}$  is larger than  $T$ . If the trace entry denotes a successful reception, the packet is forwarded, and otherwise the entry is an interpolated entry for

a missing packet and it is dropped. The times,  $T$  and  $T_{\text{near}}$ , are counted from the start of emulation and the trace, respectively. The emulator terminates once it has run for the duration of the traces.

Emulation of multi-antenna systems is achieved by using data from multiple traces. For example, to emulate the system  $\{V\} \times \{V, H\}$  we would use data from single-channel traces of  $\{V\} \times \{V\}$  and  $\{V\} \times \{H\}$ . Whenever the sender or receiver adjusts their active antenna, the emulator starts reading entries from the corresponding new trace. In the case of receive antenna selection, the emulator reads from the two traces corresponding to the active transmit antenna and the two receive antennas, and uses the entry with the highest received signal strength (RSS). Here we make the assumption that interpolated trace entries for dropped packets have a RSS of  $-95\text{dBm}$ , which is the noise floor of our radio cards.

Trace-driven emulation is deterministic in that it doesn’t use a random process for drop decisions; thus, ideally multiple runs of the same emulation experiment would produce the same outcome. In practice, different runs could experience some variation due to timing of input packets, i.e., difference between  $T$  and  $T_{\text{near}}$ . This means that the input packet may get processed using different trace entries and could be subject to different decisions on whether it will be received or dropped. We evaluated this variation by comparing packet loss between measured and emulated packet streams, computed in 100ms windows. We found that 98% of these windows were less than 4% different. Furthermore, we computed the total number of packet losses of entire traces and found that the mean difference between measured and emulated was 0.05% with a 0.04 standard deviation. These differences are negligible for our purposes of evaluating packet delivery performance.

#### 5. CPP evaluation using emulation

We used the traces from the flight experiments to evaluate transmit and receive antenna selection for  $2 \times 2$  systems such as that formed by dual-antenna Atheros radio cards. From the 20 channels formed by 4 transmit and 5 receive antennas, it is possible to evaluate 60 distinct  $2 \times 2$  systems ( $\binom{4}{2} \cdot \binom{5}{2}$ ). In this section, we present the emulation results.

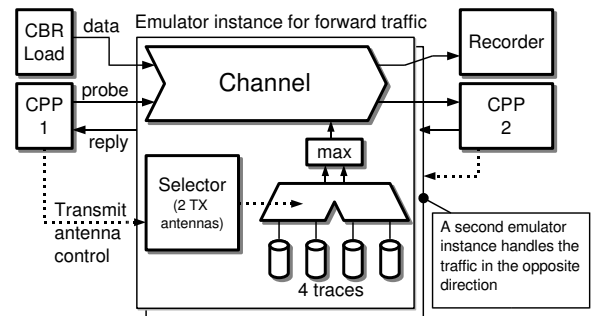


Fig. 2. Functional diagram of the emulator in a  $2 \times 2$  experiment scenario. The emulator instance shown handles one direction of traffic, while an identical one handles the other direction. Applications control the transmit antenna, while the receive antenna is determined by the “max” component based on the recorded RSSI, in order to emulate hardware receive antenna selection. In field experiments, the emulator components shown here are replaced by two instances of the Linux OS using dual antenna radio cards, and the physical wireless environment as the propagation medium.

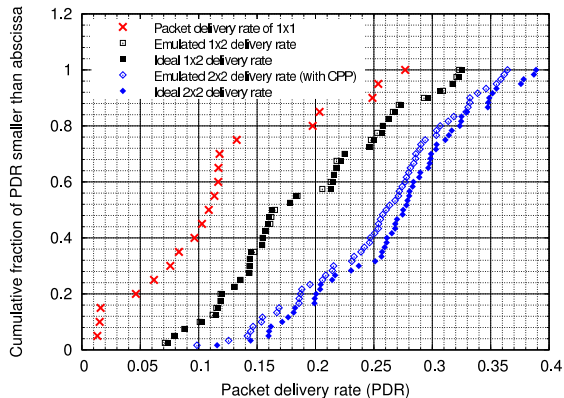


Fig. 3. Empirical cumulative distribution plots of packet delivery rate performance under emulation of  $1 \times 1$ ,  $1 \times 2$ , and  $2 \times 2$  systems, and ideal performance estimates for  $1 \times 2$  and  $2 \times 2$  systems.

We ran CPP under emulation for each of the 60  $2 \times 2$  systems, using a probing interval of 25ms. We will evaluate the effect of probing interval size in the next subsection. Along with an instance of CPP running on the sending and receiving sides, we used a CBR traffic source on the sender as the load, as depicted earlier in Figure 2. To study the performance of the  $2 \times 2$  system, we analyzed the output collected in Recorder. The emulator would reselect the active trace whenever the CPP process at either endpoint toggled the active antenna.

For comparison purposes, we estimated the ideal performance achievable from  $2 \times 2$  systems as follows. First, we computed the times at which the best antennas changed. Let us refer to the intervals between these times as *coherence intervals*. We then constructed a composite trace taking data from the best trace in each coherence interval. Even though this omniscient trace is not achievable in practice in that a real system would need instant channel information at the sender to achieve it, its packet delivery rate will serve as a performance upper bound for comparison purposes. We shall refer to the delivery rate as the “ideal performance estimate” hereon.

Figure 3 shows the performances of individual  $1 \times 1$  channels, antenna selection in  $1 \times 2$  and  $2 \times 2$  systems, and the ideal performance estimates. The  $2 \times 2$  system is the joint transmit/receive antenna selection system where the CPP-based transmit antenna selection augments the traditional receive antenna selection. The performances are expressed as packet delivery rates. This plot shows two main results: first, overall the  $2 \times 2$  systems (“emulated” and “ideal”) obtain performance higher than the  $1 \times 2$  systems, indicating that channel conditions vary slowly enough for CPP feedback to be useful. Secondly, performance of joint transmit/receive antenna selection is close to the ideal performance estimate, indicating that the CPP feedback can capture much of the available gain beyond what the  $1 \times 2$  systems achieve.

Figure 4 compares the performance of each  $2 \times 2$  system to that of its best  $1 \times 2$  and  $1 \times 1$  subsystems. For example, the performance of system  $\{V, H\} \times \{V, V_N\}$  would be plotted on the  $y$ -axis against the performance of the best of  $V \times \{V, V_N\}$  and  $H \times \{V, V_N\}$ , and the best of  $V \times V$ ,  $V \times V_N$ ,  $H \times V$  and  $H \times V_N$ . We see from this plot that 1)  $2 \times 2$  antenna selection almost never performs worse than the sub-combinations; 2) the best  $2 \times 2$  performance is 32% higher than best  $1 \times 1$ ; 3) the best  $2 \times 2$  performance is 17% higher than best  $1 \times 2$ . We note that in the last result, the additional gain due to transmit selection is

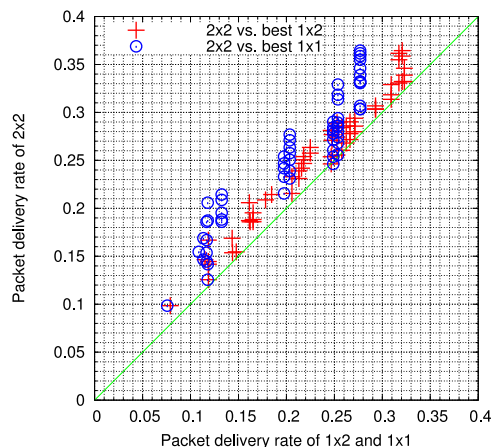


Fig. 4. This scatter-plot shows the performance of each  $2 \times 2$  system plotted against that of its best  $1 \times 2$  and  $1 \times 1$  subsystems.

similar to the  $1 \times 2$  gain, in spite of transmit selection’s inherent delay in receiving channel state information.

## 5.1. Effect of probing interval on transmit selection performance

In order to examine the effect of probing interval size  $T_P$ , we emulated a single  $2 \times 2$  system while varying  $T_P$  from 5ms to 60s. We examined the  $2 \times 2$  system with the highest packet delivery rate (0.36) and the second highest average rate of change in the best transmit antenna (1.5 per second), because it provides a high range of throughputs, and demands a high probing rate to capture the frequent best transmit antenna changes. The results are shown in Figure 5, along with the ideal performance estimate and the performance of the two  $1 \times 2$  subsystems for comparison purposes.

As we can see, there is a region between 200ms and 1s where the performance of the emulated  $2 \times 2$  system decreases from that near ideal to that of the  $1 \times 2$ , receive selection-only performance. This is a positive result in the sense that the probe interval can be as long as 200ms. Suppose for example we use a 8-byte UDP packet, which in 802.11a takes about  $159 \mu\text{s}$  to transmit at 6Mbps, including the DIFS interval and a minimal, 1-slot backoff. The amount of channel capacity taken up by two of these packets at 200ms intervals is negligibly low—less than 0.2% of channel capacity. Furthermore, the probing interval allowed by a larger, but still minimal channel overhead of 1% is 32ms, which is near the beginning of the high performance region.

## 6. CPP evaluation on a UAV testbed

In this section, we present the measurement results of CPP-based transmit antenna selection performance in the field, using a testbed that ran the unmodified software we used for the emulation in Section 5. We performed a series of flights where the UAV flew north and south along a 640-meter runway section, as depicted by the flight pattern in Figure 6 generated by an on-board GPS device. The UAV node ran the CBR packet source, transmitting to a stationary ground node. The two nodes utilized the same hardware as those in the trace collection testbed described in Section 3. The radios used channel 11 and transmitted at the 6 Mbit/s rate under 802.11g. The reason we used 802.11g instead of 802.11a as before was three-fold: 1) to obtain channel measurements at

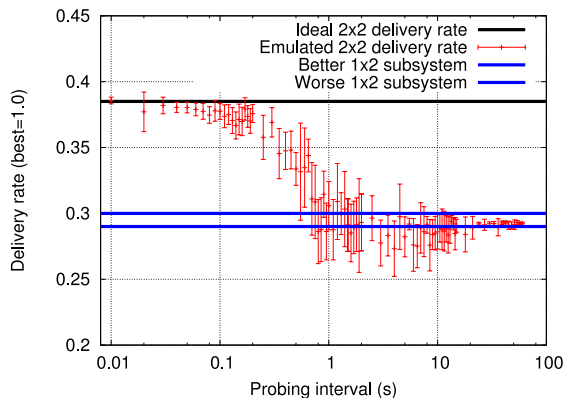


Fig. 5. Effect of probing interval on  $2 \times 2$  selection performance with CPP. Each point is an average of 10 runs. The horizontal lines indicate the ideal performance estimate and the emulated performance of the individual  $1 \times 2$  subsystems.

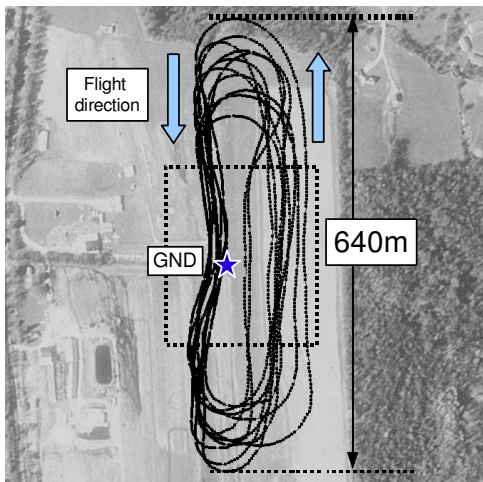


Fig. 6. The trajectory flown by the UAV during the experiment. The dotted rectangle indicates the flight data we isolated for performance measurements. The ground node is labeled “GND.”

larger distances, 2) to measure antenna usage at far ends of the flight cycles, and 3) for the purposes of a co-located LCAD experiment.

Each node was equipped with two dipole antennas—one vertical (V), and the other horizontal, oriented perpendicular to the flight path (H). We chose this arrangement on the intuition that the dipole null regions would complement each other. There are possibly other antenna combinations with more diverse performance, which we might pursue in the future. However, in this work we were attracted to the simplicity of the plain dipoles.

During the flights, we tested five major system configurations: one  $2 \times 2$  system where the nodes ran CPP, and the other four  $1 \times 1$  systems where the nodes used the four possible antenna combinations, respectively. For each system configuration, we identified straight flight segments where the UAV flew either northbound or southbound, passing the ground node. These segments are more uniform than the U-turns near the ends of the flight path and therefore are better suited for a performance comparison. These segments are highlighted in Figure 6.

Table I shows performance results for the five system

	North	(stdev)	#segments
Diversity:	79.9%	(6.254)	11
V-V:	75.6%	(6.031)	4
V-H:	32.4%	(6.951)	4
H-V:	31.4%	(8.218)	9
H-H:	47.5%	(7.732)	4
	South	(stdev)	#segments
Diversity:	82.9%	(5.101)	10
V-V:	79.4%	(14.731)	3
V-H:	33.1%	(7.392)	5
H-V:	40.9%	(3.372)	7
H-H:	66.4%	(4.938)	4

TABLE I. Delivery rate performance for four single-antenna configurations and one antenna selection run.

configurations, computed from individual flight segments. The performance metric we focus on is the packet delivery rate, shown as a percentage of packets transmitted, and the sample deviation. The table also includes the number of flight segments used to compute each value.

According to these results, the performance with CPP-based transmit antenna selection, indicated by the diversity numbers in the table, is on average 5.7% better than the best static antenna pair. However, assuming normally distributed samples, the confidence of this conclusion is only 51%. One possible reason that the use of antenna diversity did not obtain a more significant gain in this particular field experiment is the relatively low altitude of the UAV. In particular, as the UAV approaches the ground node and the V-V antenna signal drops due to aligned null regions, but the distance also decreases and offsets this loss of signal. Another issue unique to these field results is that the CPP and the four individual antenna runs were measured on separate flights, introducing variations due to flight path discrepancies that were not present in the emulation data set. Thus, obtaining a more statistically significant result would require enough additional flight time to reduce the flight path variation. We plan to perform further such experiments in the future.

Figure 7 shows a more detailed comparison of the five system configurations using a plot of delivery rate versus distance. Here we can see that the performance with CPP is consistently near best of the five, whereas all of the static antenna settings have poor performing regions. We examine the CPP performance in more detail in Figure 8, which shows aggregate signal strength, delivery rate, and antenna usage data. As we can see from the antenna usage curve, the system tends to use the H-H pair at closer distances, while it spends an increasing fraction of the time on the V-V pair as the distance grows.

To further demonstrate the CPP operation, we compare its performance directly with that of V-V by plotting in Figure 9 the raw time-series performance of two individual southbound flight segments. We can clearly see the throughput drop in the middle of the V-V trace (Figure 9(a)), which occurs as the UAV flies over the ground node, bringing the V-V antennas into rough co-linear alignment. That throughput drop is absent in the CPP trace (Figure 9(b)), while there is a significant antenna usage shift toward the H-H pair.

## 7. Conclusion

In this paper we presented the first experimental results of joint transmit/receive antenna selection in outdoor mobile 802.11 networks using a UAV testbed. Our contributions are:

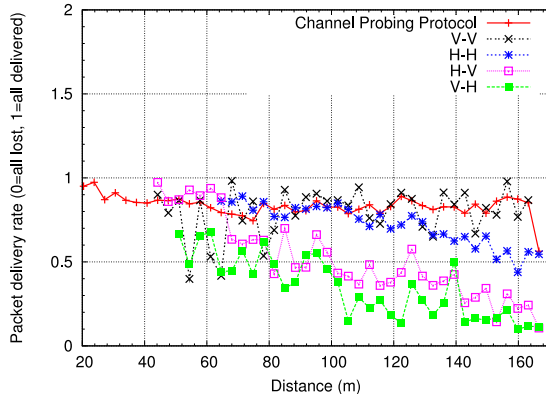


Fig. 7. A plot of delivery rate performance against distance between the UAV and ground node. We computed average delivery rates and distances over 50ms intervals, sorted them among 50 distance bins, and then plotted the averages within each distance bin.

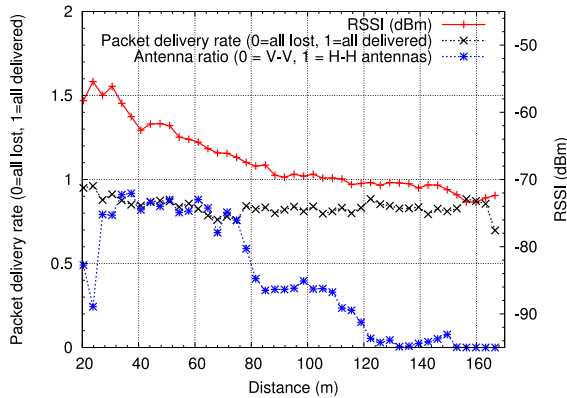
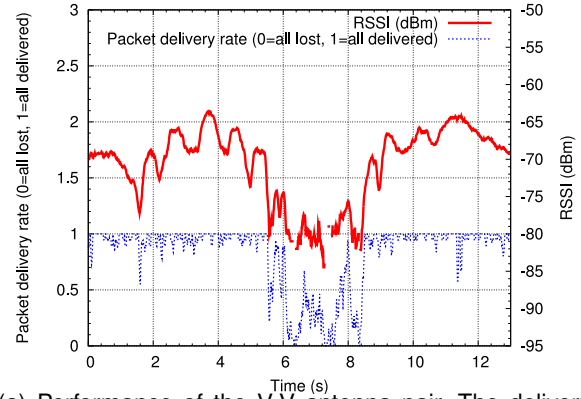


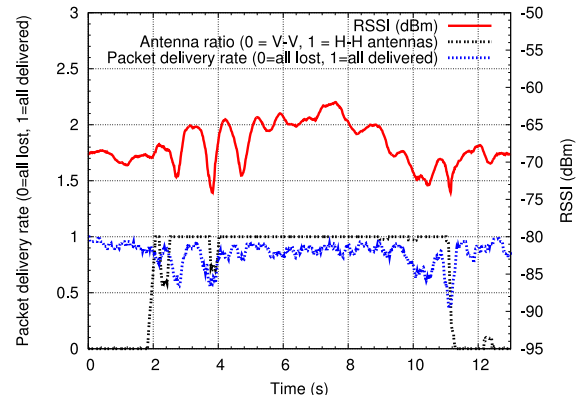
Fig. 8. Received signal strength, delivery rate, and antenna usage of CPP over distance (shown as a ratio between V-V and H-H only), computed from aggregate flight data. We computed averages for each metric over 50ms intervals, sorted them among 50 distance bins, and plotted averages from each distance bin.

- A set of high resolution, multi-channel packet loss and signal strength traces of UAV-to-ground communication.
- A trace-driven multi-antenna channel emulator.
- Emulation and experimental evaluation of antenna selection, which have shown that even with just two antennas per node, there are many antenna configurations for which transmit antenna selection achieves a performance improvement.
- A transmit antenna selection mechanism based on a link-layer feedback protocol.

The positive evaluation results prove three key points. 1) Different antennas can experience fading with enough statistical independence to let antenna selection obtain a performance gain. 2) For the UAV mobile network environment we examined, these fading conditions indeed change slowly enough for a relatively low-rate link-layer feedback protocol to adapt. 3) The link-layer feedback appears to work, i.e., the channel state information it measures translates into improved packet delivery performance, which is what the application really cares about. Based on these points, we conclude that transmit antenna selection is already a practical technique for achieving significant performance gain, even on commodity hardware and without changes to the 802.11 protocols.



(a) Performance of the V-V antenna pair. The delivery rate for this segment was 82%.



(b) Performance with CPP protocol. The delivery rate for this segment was 85%.

Fig. 9. Raw performance traces from individual southbound fly-by segments using CPP, and static V-V antennas. We selected the two fly-by segments with the closest average distance and altitude.

## References

- [1] "Senior Telemaster R/C Airplane by Hobby Lobby International, Inc." <http://www.hobby-lobby.com/srtele.htm>, 2006.
- [2] D. Aguayo, J. Bicket, S. Biswas, G. Judd, and R. Morris, "Link-level Measurements from an 802.11b Mesh Network," in *SIGCOMM 2004*, Aug. 2004.
- [3] Carl B. Dietrich, Jr., K. Dietze, J. R. Nealy, and W. L. Stutzman, "Spatial, Polarization, and Pattern Diversity for Wireless Handheld Terminals," *IEEE Transactions on Antennas and Propagation*, vol. 49, no. 9, pp. 1271–1281, September 2001.
- [4] C.-M. Cheng, P.-H. Hsiao, H. T. Kung, and D. Vlah, "Performance Measurement of 802.11a Wireless Links from UAV to Ground Nodes with Various Antenna Orientations," in *15th International Conference on Computer Communications and Networks (ICCCN 2006)*, Arlington, VA, USA, Oct. 2006.
- [5] —, "Maximizing Throughput of UAV-Relaying Networks with the Load-Carry-and-Deliver Paradigm," in *IEEE Wireless Communications and Networking Conference (WCNC 2007)*, Hong Kong, Mar. 2007.
- [6] T. Fujisawa, J. Hasegawa, K. Tsuchie, T. Shiozawa, T. Fujita, T. Saito, and Y. Unekawa, "A Single-Chip 802.11a MAC/PHY With a 32-b RISC Processor," *IEEE J. Solid-State Circuits*, vol. 38, no. 11, pp. 2001–2009, Nov 2003.
- [7] A. Hottinen and R. Wichman, "Transmit Diversity by Antenna Selection in CDMA Downlink," in *IEEE 5th International Symposium on Spread Spectrum Techniques and Applications*, September 1998.
- [8] J. G. Proakis, *Digital Communications*, 2nd ed. McGraw-Hill, 1989, pp. 721–725.
- [9] S. Sanayei and A. Nosratinia, "Antenna Selection in MIMO Systems," *IEEE Communications Magazine*, vol. 42, no. 10, pp. 68–73, October 2004.
- [10] A. M. D. Turkmani, A. A. Arowojolu, P. A. Jefford, and C. J. Kellet, "An Experimental Evaluation of the Performance of Two-Branch Space and Polarization Diversity Schemes at 1800 MHz," *IEEE Transactions on Vehicular Technology*, vol. 44, pp. 318–326, March 1995.